ACTUATORS

A mechanics-based approach to realize high–force capacity electroadhesives for robots

David J. Levine, Gokulanand M. Iyer, R. Daelan Roosa, Kevin T. Turner*, James H. Pikul*

Materials with electroprogrammable stiffness and adhesion can enhance the performance of robotic systems, but achieving large changes in stiffness and adhesive forces in real time is an ongoing challenge. Electroadhesive clutches can rapidly adhere high stiffness elements, although their low force capacities and high activation voltages have limited their applications. A major challenge in realizing stronger electroadhesive clutches is that current parallel plate models poorly predict clutch force capacity and cannot be used to design better devices. Here, we use a fracture mechanics framework to understand the relationship between clutch design and force capacity. We demonstrate and verify a mechanics-based model that predicts clutch performance across multiple geometries and applied voltages. On the basis of this approach, we build a clutch with 63 times the force capacity per unit electrostatic force of state-of-the-art electroadhesive clutches. Last, we demonstrate the ability of our electroadhesives to increase the load capacity of a soft, pneumatic finger by a factor of 27 times compared with a finger without an electroadhesive.

INTRODUCTION

The ability to program the mechanical stiffness of robotic systems has led to many advances and increased the performance of prosthetics (*1*), walking robots (*2*), active origami structures (*3*–*5*), and human exoskeletons (*6*). Clutches are a common approach for programming stiffness and operate by mechanically connecting and disconnecting elements of different stiffness. Rotational clutches in robots can be activated to block force, control energy transfer between mechanical elements, and enable discrete stiffness tuning (*7*, *8*). However, rotational clutches are restricted to rotational joints and are made from rigid materials (*1*, *9*–*11*), which makes them incompatible with applications that require stretchability or in-plane mechanical programming. For these applications, soft materials with programmable stiffness have been developed to modulate stiffness in soft or stretchable robotic systems. These materials enable transformations between complex, preprogrammed shapes (*12*), robotic fish with increased swimming efficiencies (*13*), and mechanically patterned grippers for gentle object manipulation (*14*). The ability to program large changes in mechanical stiffness in real time, however, has been a challenge with current soft stiffness tuning mechanisms, which consume large amounts of power, require phase changes, actuate in seconds to minutes, or have low strength (*15*, *16*).

A promising technology for modulating stiffness in soft or flexible systems is an electroadhesive clutch (*15*). In contrast to rotational clutches, electroadhesive clutches are composed of one or more thin, compliant, conductive, overlapping electrodes separated by a dielectric layer (Fig. 1A). When a voltage is applied between the conductive surfaces, the opposing charges on each electrode are attracted to one another, resulting in electroadhesion (*17*, *18*). The electrostatic force produced at the contact interface can prevent sliding and increases in the in-plane stiffness (*15*). When the clutch is loaded in tension or by an external bending moment, each electrode is pulled parallel to its length and away from the opposing electrode so that, in the absence of an applied voltage, they slide relative to each other. Therefore, when no voltage is applied, the unactivated stiffness is determined by the materials surrounding the clutch (Fig. 1B). Electroadhesives are lightweight (<1 g) because of the small thickness of the electrodes, and the stiffness changes occur in milliseconds. Moreover, electroadhesive clutches are low cost and easy to fabricate and consume small amounts of power (<1 mW) when fully charged. As a result, many electroadhesive clutches have been developed in recent years for programming stiffness changes in a variety of applications, including wearable haptic interfaces for virtual reality and robotic teleoperation (*19*–*21*), robotic exoskeletons for ankle assistance during walking tasks (*22*, *23*), fingered gripping systems (*24*), modular robotic teams (*25*), shape locking of pneumatic actuators (*26*), and electrostatic zipping actuators (*3*).

However, despite the proliferation of electroadhesive clutch designs in numerous applications where stiffness control is required, current electroadhesive clutches suffer from force capacities (FCs) below those of other materials with an electrically tunable stiffness, such as electrothermal and electrochemical systems (*15*). The FC is the force above which the clutch would fail or slip. Clutches with increased FCs can reduce the applied voltage needed to achieve a target force, shrink device dimensions, and increase the achievable stiffness range. These benefits would make electroadhesive clutches more compatible with off-the-shelf electronics and both macroscale and microscale robotic systems. To achieve this, the FC of electroadhesive clutches must be increased by a factor of 10 compared with what is achievable today (*20*).

Current electroadhesive clutches rely on high operating voltages (typically >300 V) and large contact areas to achieve larger FCs, but an incomplete understanding of clutch mechanics has prevented current designs from achieving their full potential. To date, clutches have been designed using a simple electroadhesion model based solely on electrostatic parallel plate theory and Coulombic friction to predict the FC (*27*). Although simple in nature, this model does not accurately predict real-world performance in many cases,

Department of Mechanical Engineering and Applied Mechanics, University of Pennsylvania, Philadelphia, PA 19104, USA.
*Corresponding author. Email: kturner@seas.upenn.edu (K.T.T.); pikul@seas.upenn.edu (J.H.P.)

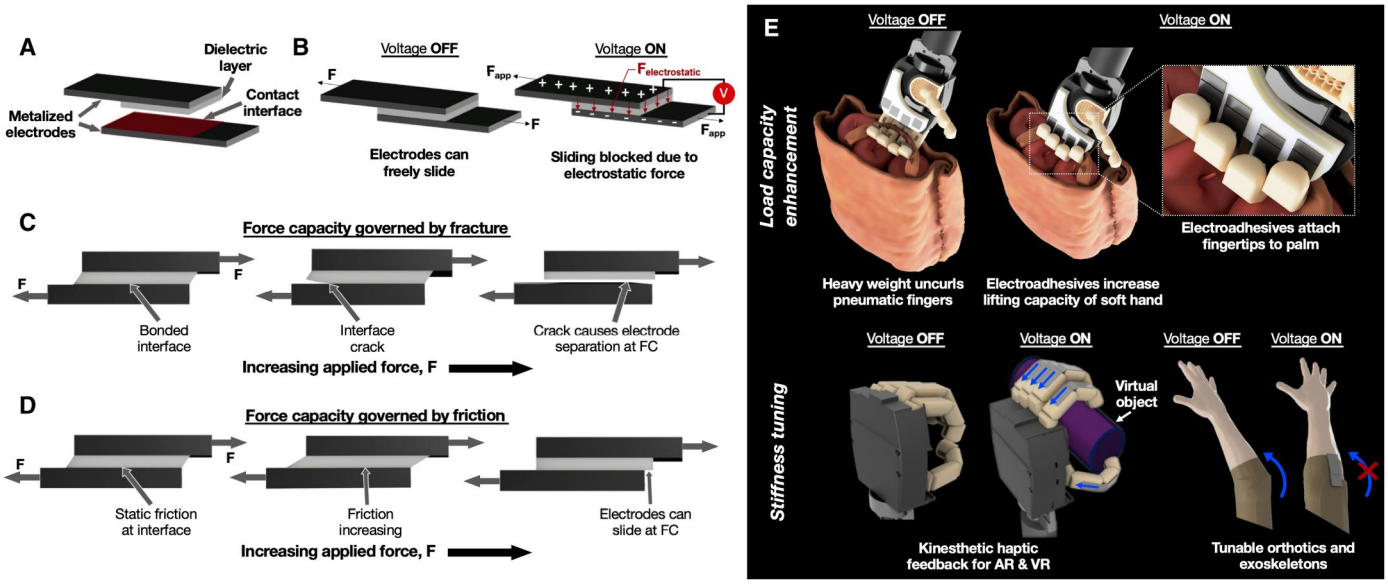

Fig. 1. Electroadhesive clutch materials, operation, applications, and design. (**A**) Electroadhesive clutches that use Coulombic electroadhesion are composed of two compliant, metallized electrodes separated by an insulating dielectric layer with relative permittivity κ. The contact area between the dielectric and the bottom electrode is denoted in red. (**B**) Electroadhesive clutch operation. In the off state, contact is made between the clutch surfaces, but they are not adhered and can slide freely past one another (left). In the on state, the two electrodes are held together by electrostatic forces, and sliding is blocked at the contact interface (right). (**C**) Electroadhesive FCs are governed by interface fracture mechanics. First, a crack initiates at the edge of the contact interface (left), which grows as the load applied to the clutch increases (middle). At its FC, the crack propagates through the whole interface, and the surfaces of the clutch separate (right). (**D**) Previous understanding of electroadhesive FCs was based on parallel plate theory and friction. Using this approach, static friction from electrostatic attraction holds the electrodes together (left), which increases as the load applied to the clutch increases (middle). At its FC, a slip event occurs, and the electrodes slide past one another (right). (**E**) Applications of electroadhesive clutches in robotic systems. Electroadhesive clutches can resist tensile loads to increase the holding capacity of a soft robotic gripper (top), tune the stiffness of a soft actuator or wearable device to provide kinesthetic haptic feedback to simulate the feeling of a virtual object (bottom left), or tune the bending stiffness of an orthotic, splint, or exoskeletal device (bottom right). AR, augmented reality; VR, virtual reality.

because it does not account for nonuniform stresses and failures that occur due to the initiation and propagation of interface crack (i.e., fracture-based failure) (Fig. 1C) (*28*–*34*). There is, therefore, a need for models that accurately capture electroadhesive behavior and that, in turn, will enable the design of stronger, smaller, and lower-voltage clutches for programming stiffness or adhesion.

We present an experimentally validated fracture mechanics–based model that describes the relationship between clutch design and maximum FC and show that using this model can enable electroadhesive clutches with notable improvements in FC. Our model correctly predicts clutch performance over a wide variety of geometries and applied voltages, unlike the widely used parallel plate equation (Fig. 1D). Using this understanding, we demonstrate that the performance of most electroadhesive clutches can be improved by simply changing their geometry, i.e., shape and thickness. On the basis of our design criteria, we built a Coulombic electroadhesive clutch with the highest FC per applied electrostatic force, outperforming the next highest-performing clutch by a factor of 63×. Last, we demonstrate the ability of our optimized electroadhesives to increase the load capacity of a soft robotic finger by a factor of 27×. By doing so with traditional dielectrics and electrode materials, we demonstrate the power of our mechanics-based design methodology to increase clutch performance without relying on expensive materials or intensive manufacturing processes, making our approach optimal for widespread adoption by robotics researchers. This fundamental understanding of clutch mechanics and improved FC will enable smaller and stronger clutches for programming the mechanical properties of robotic systems.

RESULTS

Analytical modeling

To predict FC, we modeled electroadhesive clutches as bonded lap joints. Lap joint models assume that the adhesive layer is loaded in shear (*35*–*38*), undergoes failure via fracture upon reaching its FC (*39*), and is linear elastic before failure (*28*, *29*). Because the same assumptions apply to electroadhesive clutches, their mechanics are akin to those of adhesively bonded lap joints. Although other fracture-based models exist for electroadhesive lap joints, they assume the electroadhesive to have no stiff electrode backing, which leads to a different failure mechanism compared with the clutches in this work (*40*). Using a fracture-based, analytical model of bonded lap joints (*28*, *29*), the FC of an electroadhesive clutch can be expressed as

$$\mathrm{FC} = \beta\sqrt{2G_c}\sqrt{\frac{A}{C}} \tag{1}$$

where C is the overall compliance of the clutch system, A is the contact area between electrodes (red area in Fig. 1A), β is a constant (assumed to be 1 in this work), and G_C is the critical strain energy release rate, which describes the adhesion at the interface and is not a function of clutch geometry or compliance (*31*). We define

compliance as the axial displacement of a clutch with no slipping divided by the applied force. Modifications to compliance through shape change (*28*, *29*, *34*) and geometric confinement (*27*) have been previously shown to increase FC for nonelectrically controlled adhesive joints loaded in shear. Note, however, that such increases in FC reported in (*27*) could not be explained by the parallel plate friction model described in Eq. 2, which was the model used to predict electroadhesive FC in that study. Our model assumes that FC is the force at which the strain energy release rate G is equal to a critical strain energy release rate, G_C. The critical strain energy release rate can be thought of as the interface toughness or interface fracture energy required to separate the clutch surfaces. In an electroadhesive clutch, G_C is directly proportional to the square of the applied voltage (V^2), which is a relationship predicted by parallel plate electrostatic theory (*41*). This model has notable differences from the clutch FC predicted by parallel plate models, which is

$$\mathrm{FC}_{\mathrm{pp}} = \mu F_{\mathrm{el}} = \mu \frac{\varepsilon_0 A (\kappa V)^2}{2d^2} \tag{2}$$

where F_{el} is the electrostatic force, μ is the coefficient of friction between dielectric and electrode, ε_o is the permittivity of free space, A is the contact area, κ is the relative permittivity, V is the applied voltage, and d is the thickness of the dielectric. First, according to Eq. 1, FC is directly proportional to $G_C^{1/2}$, which leads to a direct scaling with V and not V^2, as Eq. 2 predicts. Next, our model assumes FC to be governed by adhesion and interface fracture (Fig. 1C), whereas the FC of parallel plate models depends on static friction (Fig. 1D). Last, Eq. 2 is independent of the clutch compliance (C) and only considers A and d to be relevant geometric parameters that contribute to FC. In contrast, our model takes C into account, which includes not only the contact, or overlap region but also the free, noncontacting regions of the clutch, along with the contact area (A). The total compliance must be considered in a predictive model, because each clutch will undergo deformation in its overlap region and free regions, which all contribute to nonuniform shear and peel stresses that cause electrode separation at FC (*35*–*38*).

We denote the quantity $(A/C)^{1/2}$ as the geometric stiffness parameter (GSP), which accounts for the overall clutch compliance and electroadhesive contact area. Figure 2A shows the spring-based model for overall clutch compliance. To satisfy the linear elastic assumption required by Eq. 1, we measured the clutch compliance at small strains (1 to 1.5%) (fig. S1). The electroadhesive joint is split into two distinct regions. These include (i) the overlap region, where the electrodes are adhered and both the dielectric and electrode layers undergo deformation, and (ii) the free regions away from the contact, where only the electrodes undergo deformation. In the overlap region, the dielectric and two adherends are treated as springs in parallel, and their axial compliance is

$$C_{\mathrm{overlap,axial}} = \frac{L}{w}\left[\frac{1}{2E_e t + E_d d}\right] \tag{3}$$

where E_e is the Young's modulus of the electrodes, E_d is the Young's modulus of the dielectric, t is the thickness of the electrodes, d is the thickness of the dielectric layer, w is the width of the overlap region, and L is the length of the overlap region. For the single lap shear configuration, there is eccentricity in the loading path, which results in the joint being loaded by a moment that leads to bending and shear deformation of the dielectric. However, because the thickness of the dielectric is substantially smaller than the overlap length ($d << L$) in the clutches presented here, we neglect both the shear and bending compliance. The compliance of the two free regions, which are loaded axially, is

$$C_f = \frac{L_f}{E_e w t} \tag{4}$$

where L_f is the length of the free region. The experimentally measured compliance of the testing machine (C_{machine}) is also included. Adding these compliances in series, the total system compliance is

$$C_{\mathrm{total}} = \frac{L}{w(2E_e t + E_d d)} + \frac{2L_f}{E_e t w} + C_{\mathrm{machine}} \tag{5}$$

which is similar to the system compliance used in (*29*). Figure S2 shows reasonable agreement between the measured and predicted clutch stiffnesses k, which is equal to the reciprocal of the compliance ($1/C_{\mathrm{total}}$). Last, we combined Eqs. 1 and 5 to find an expression for electroadhesive FC. This model illustrates that the electroadhesive FC depends on material and geometric parameters as well as contact area and applied voltage, so all of these parameters must be considered in clutch design.

Figure 2 (B to D) summarizes the effect of clutch shape and applied voltage on electroadhesive FC. Figure 2B shows the FC as a function of clutch width. The lines of constant area were calculated using the model with a G_C value corresponding to our 200-V FC experiments (G_C = 4.71 J m^{-2}), and the lines of constant voltage were calculated using G_C values corresponding to our 125-, 150-, and 200-V FC experiments (G_C = 1.77, 2.76, and 4.71 J m^{-2}). These G_C values were determined by performing a linear regression on our GSP versus FC experimental data at 125, 150, and 200 V, where the slope was equal to $(2G_C)^{1/2}$. G_C was determined from the best fit lines: 125 V [G_C = 1.77 J m^{-2}, coefficient of determination (R^2) = 0.98], 150 V (G_C = 2.76 J m^{-2}, R^2 = 0.99), and 200 V (G_C = 4.71 J m^{-2}, R^2 = 0.98). The map in Fig. 2C assumes 200-V operation and shows FCs for overlap lengths (L) and widths (w) ranging from 0 to 80 mm. Overall, increasing the GSP of an electroadhesive clutch (decreasing total compliance and increasing contact area) increases the FC. Our model showed that holding the contact area constant but changing the clutch shape leads to changes in FC as the clutch compliance also changes [FC α $(A/C)^{1/2}$]. This contradicts the predictions of parallel plate electrostatic models, which do not account for joint stiffness, indicate that FC α A, and suggest that FC should be constant if A is fixed. Figure 2 (B and D) shows lines of constant area to illustrate this point. To reduce the contact area of any electroadhesive clutch without decreasing its FC, its overlap width can be increased and its joint length reduced (Fig. 2C). Moreover, Fig. 2D shows how voltage influences FC, where G_C is proportional to V^2. Lines corresponding to 125, 150, and 200 V (G_C = 1.77, 2.76, and 4.71 J m^{-2}) are shown, which were determined by fitting the model to the experimental data. This relationship shows that the applied voltage can be reduced without reducing the electroadhesive FC by decreasing joint compliance and/or increasing contact area. Overall, the contour maps show the combined influence of compliance, contact area, and applied voltage on electroadhesive

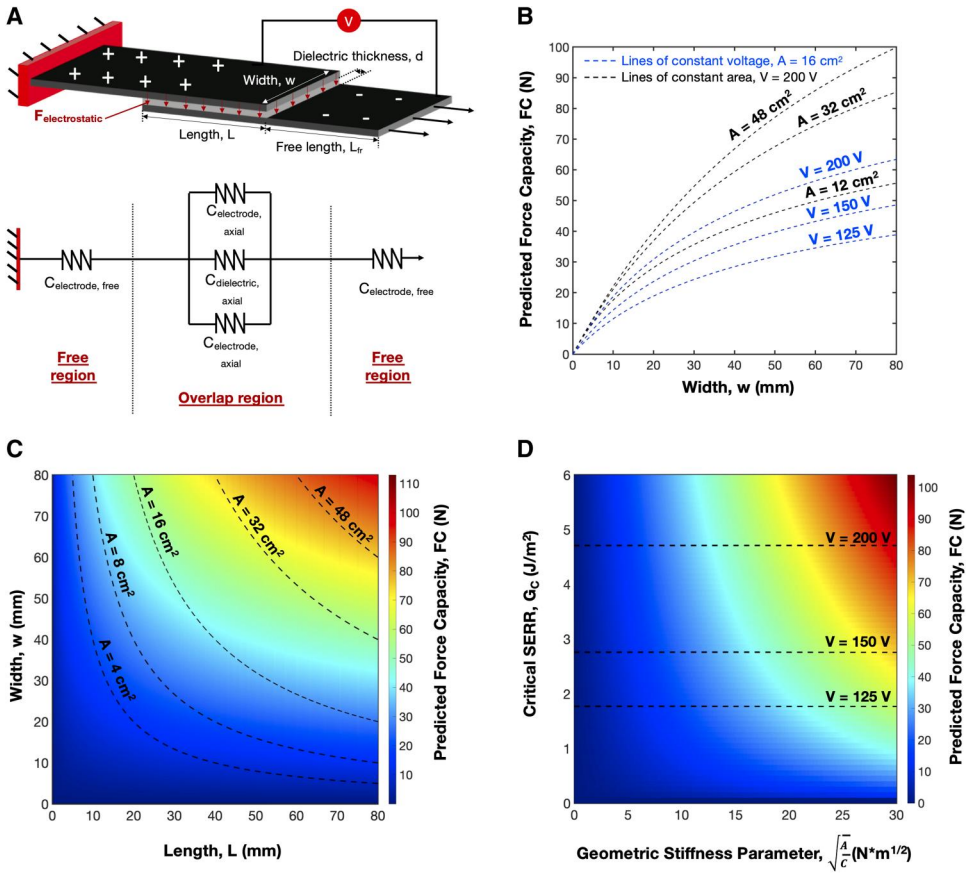

Fig. 2. Predictions of the analytical model of electroadhesive clutch joint stiffness and FC. (**A**) A schematic of an electroadhesive clutch with important geometric and material parameters labeled (top) and the representative spring network used to predict total joint compliance and electroadhesive FC (bottom). (**B**) FC as a function of clutch width predicted by the model. The lines of constant area were calculated using our model with a G_C value corresponding to our 200-V FC experiments, and the lines of constant voltage were calculated using G_C values corresponding to our 125-, 150-, and 200-V FC experiments. All lines of constant area (black) represent clutches operated at a set voltage of $V = 200$ V, and all lines of constant voltage (blue) represent clutches with a set area of $A = 16$ cm^2. (**C**) A design map showing electroadhesive FCs for different electroadhesive joint lengths and joint widths. The dotted lines represent electroadhesives with constant contact areas of $A = 4$ to 48 cm^2. (**D**) A design map of predicted electroadhesive FCs for different GSPs and critical strain energy release rates (G_C), which correspond to different voltages. The dotted horizontal lines of constant voltage were calculated using G_C values corresponding to our 125-, 150-, and 200-V FC experiments. All model predictions assume geometries and material properties that match those of the clutches that were experimentally tested.

FC, which all need to be considered in the design to optimize a clutch for a set of design constraints.

Experimental validation

To validate our analytical model for the FC of an electroadhesive clutch, we performed mechanical tests of electroadhesives with a variety of compliances (see Materials and Methods for details; setup is shown in fig. S3). For each electroadhesive, we measured FC, stiffness (at small strains of 1 to 1.5%), and the maximum possible contact area. First, we assessed the validity of GSP as a predictive variable for clutch FC. Figure 3A shows that there is a linear relationship between the calculated GSP and measured FC, where the $(2G_C)^{1/2}$ slope matches the prediction in Eq. 1. The slope of the best fit line for the 125-, 150-, and 200-V datasets increased by the same degree as the voltage increased: 1.63× for 125 to 200 V (1.88% below the expected 1.6×) and 1.31× for 150 to 200 V (1.75% below the expected 1.33×) for clutches with the same geometric parameters, which agreed with the predicted FC α V relationship.

Next, we measured the influence of clutch stiffness on electroadhesive FC by changing the clutch aspect ratio as we maintained a constant contact area of 16 cm^2. Figure 3B shows that the FC increases with increasing width, which corresponds to a decreased compliance as the length shrinks to keep the area constant (blue data). The electroadhesives had a fixed free length of 24 mm, a fixed electrode thickness of 127 μm, an applied voltage of 200 V, and a set dielectric thickness of 14 μm, so that the electrostatic pressure (E_p) was constant. The electrostatic pressure is the total electrostatic force divided by the contact area ($E_p = F_{el}/A$). Figure 3C shows electroadhesive FC as a function of width for clutches with thicker electrodes ($t = 254$ μm). These clutches (shown in black) had the same parameters used in the initial test ($A = 16$ cm^2, $V = 200$ V, $d = 14$ μm, and $L_f = 24$ mm, with varying L and w), but they showed larger FCs compared with the specimens of $t = 127$ μm (shown in blue) because of the decrease in total compliance, even at a fixed contact area. For both experiments, the measured data match the predicted values from the analytical model. These results show that the electroadhesive FC can vary substantially

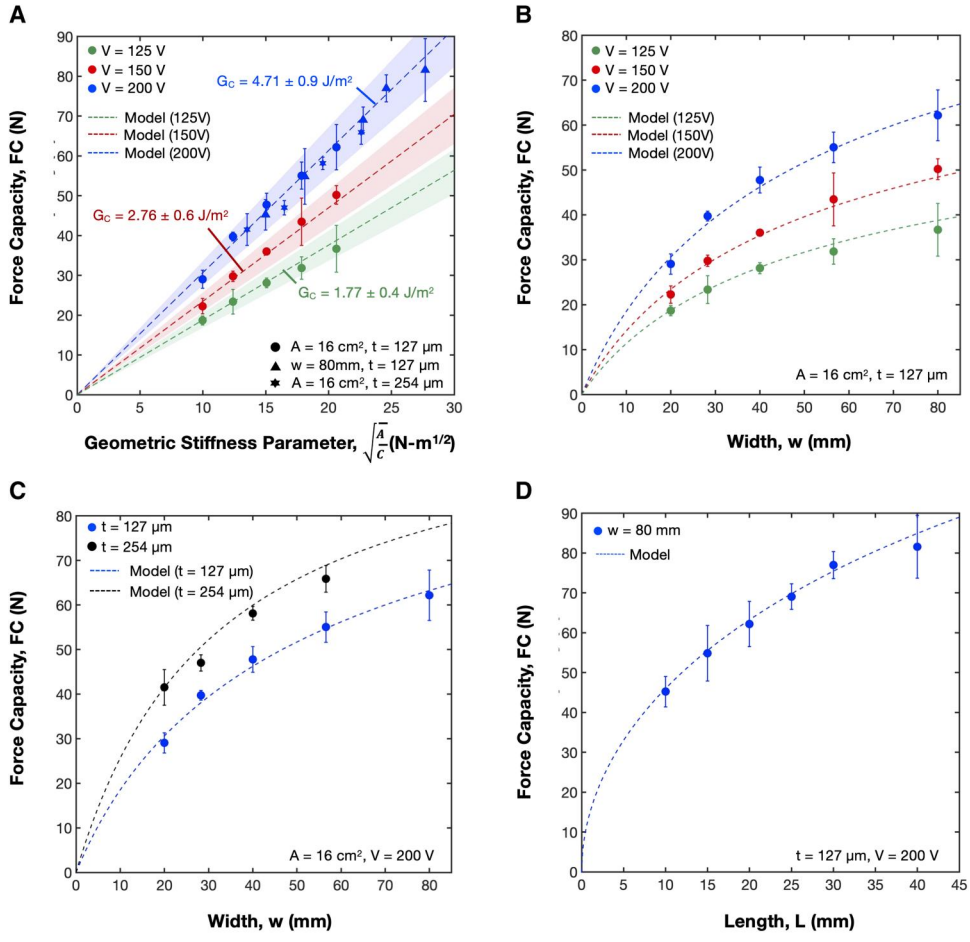

Fig. 3. Experimental validation of the analytical model and an exploration of electroadhesive clutch stiffness on FC. (**A**) Measured electroadhesive FC as a function of the GSP. Each data point indicates a different electroadhesive clutch design, with $n = 3$ clutches tested per data point. The error bars indicate 1 SD above and below each measured FC value. The green, red, and blue dotted lines indicate the model-predicted values of electroadhesive FC with $G_C = 1.77$ J m^{-2} for the 125-V data, 2.76 J m^{-2} for the 150-V data, and $G_C = 4.71$ J m^{-2} for the 200-V data. The green, red, and blue shaded regions indicate a 20% deviation in G_C from the fitted parameters. (**B**) Measured electroadhesive FC versus electroadhesive joint widths for clutches tested with different operating voltages (V) at a set contact area of 16 cm^2, with all other design parameters fixed. The green dotted line indicates the model's predictions for 125-V operation, the red dotted line indicates the model's predictions for 150-V operation, and the blue dotted line indicates the model's predictions for 200-V operation. (**C**) Measured electroadhesive FC as a function of electroadhesive clutch widths for clutches with different electrode thicknesses (t) at a set contact area of 16 cm^2, with all other design parameters fixed. The blue dotted line indicates the model's predictions for $t = 127$ μm electrodes, and the black dotted line indicates the model's predictions for $t = 254$ μm electrodes. (**D**) Measured electroadhesive FC as a function of electroadhesive clutch lengths with all other design variables fixed. The blue dotted line indicates the model's predictions for 200-V operation.

under a constant area, which contradicts prior parallel plate models and reinforces the importance of considering the clutch compliance in device design.

To investigate the effect of simultaneous changes in both electroadhesive clutch compliance and contact area on FC, we tested electroadhesives with the same electrode and dielectric thicknesses (t = 127 μm, d = 14 μm, and L_f = 40 mm) at an applied voltage of V = 200 V but held overlap width constant at w = 80 mm and varied the overlap length L from 10 to 40 mm, which corresponded to contact areas ranging from 8 to 32 cm^2 (Fig. 3D). We observed a nonlinear increase in electroadhesive FC at increased overlap lengths, which corresponds with the simultaneous increase in contact area and clutch compliance predicted by the analytical model. This dependence of FC on overlap length arises from the clutch's load train compliance (free region compliance and machine compliance), which has been previously shown to affect FC for adhesive specimens that undergo electrode separation at FC (*42*), like our electroadhesive clutch designs (fig. S1).

Last, the clutches operated at different voltages not only followed the trend predicted by the model (FC α V) but also showed the same predicted nonlinear increase in FC for larger clutch widths and shorter clutch lengths (Fig. 3B). Overall, our experimental data for FC at a variety of clutch compliances and contact areas are in good agreement with the analytical model.

Soft actuator demonstration

Strong electroadhesives can modulate the stiffness and strength of robotic systems, but for many soft robotic applications, such as gripping, the elastomer compliance that enables robust damage-free interactions with fragile objects (*43*) also results in reduced load-carrying capabilities. For example, we show a custom pneumatically actuated soft hand that can carry one 0.2-kg apple with two inflated

fingers (Fig. 4A). When the same fingers are loaded with a 1.8-kg bag of apples, the fingertips bend away from the palm, and the hand drops the load (movie S1). We show that strong electroadhesives attached to soft robotic fingertips can increase their load-carrying capacity by mechanically connecting the fingertip to the palm (Fig. 4B and additional details in fig. S4), which allows the same robotic hand to lift a 1.8-kg bag of apples with one finger without dropping it (movie S1). When the electroadhesive is not activated, a finger inflated to 30 kPa can sufficiently bend to touch the palm under zero load but is easily uncurled by a small 0.1-kg mass, which

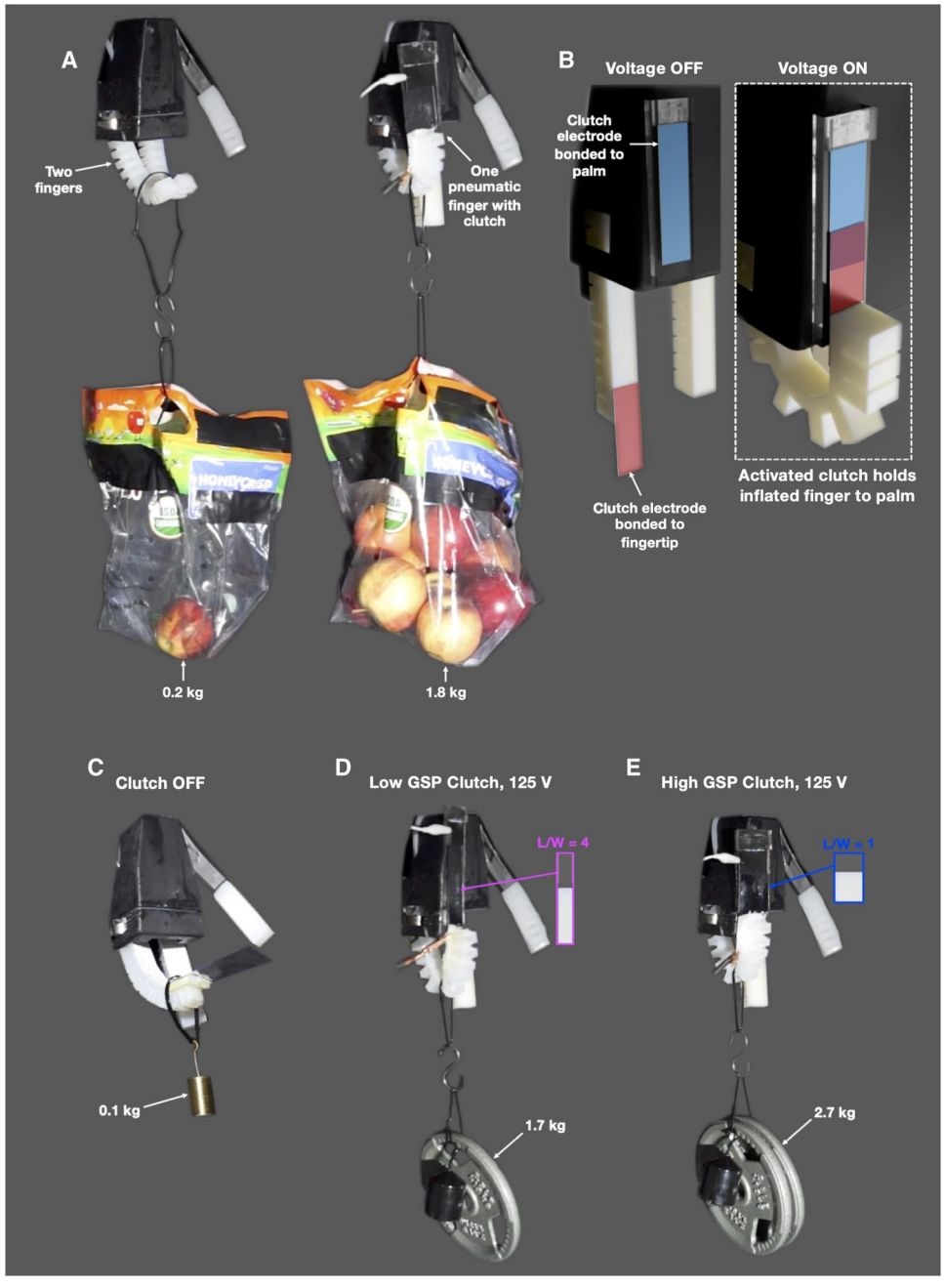

Fig. 4. Using an electroadhesive clutch to increase the load capacity of a soft robotic hand. (**A**) A soft robotic hand required two fingers (each inflated to 30 kPa) to successfully hold a bag containing one apple weighing 0.2 kg without dropping it. By using a clutch to mechanically anchor one of the hand's fingers to its palm, the hand successfully held a full bag of apples weighing 1.8 kg with only one finger, without increasing the input pneumatic pressure. (**B**) A schematic of the soft finger setup. The pneumatic finger was attached to a rigid palm (black) and was connected to an air tube for inflation. One clutch electrode was attached to the palm (blue), and the other was attached to the fingertip (red). The finger was anchored to the palm upon inflation of the finger and activation of the clutch. (**C**) Determining the load capacity of a finger without a clutch. As a control, a 0.1-kg mass uncurled a soft finger pressurized to 30 kPa. (**D**) Increasing finger load capacity with a low-GSP electroadhesive clutch. Upon activation at 125 V, this clutch enabled the same finger to hold 1.7 kg, a 17× increase compared with the control. (**E**) Increasing finger load capacity with an increased GSP electroadhesive clutch. Upon activation at 125 V, this clutch enabled the same finger to hold 2.7 kg at failure, a 27× increase compared with the control.

therefore represents the load capacity of the simple finger (Fig. 4C). To use the electroadhesive, we inflated the finger to 30 kPa, which brought the electrodes into a parallel configuration. After turning on the voltage and lightly pressing the electroadhesive electrodes into contact, the two electrodes became adhered. Mass was then added to the finger directly underneath the electroadhesive. A secondary attachment feature (zip tie) was used to ease the placement of mass on the finger. The zip tie was not tightened to grip the finger, so when the finger was overloaded, the mass and zip tie easily slipped off. An electroadhesive with L = 80 mm, w = 20 mm, V = 125 V, t = 127 μm, d = 14 μm, and L_f = 24 mm increased the finger′s load capacity from 0.1 to 1.7 kg, at which point the electrodes separated (movie S2). For this electroadhesive design operated at 125 V, our model predicts an FC of 1.85 kg, which is only 8.1% larger than the measured FC. We also tested an electroadhesive with increased GSP to further increase the finger′s FC. The stronger electroadhesive had a larger overlap width (w = 40 mm) and smaller overlap length (L = 40 mm), with the other design variables fixed (V = 125 V, d = 14 μm, t = 127 μm, and L_f = 24 mm). This electroadhesive increased the finger′s FC to 2.7 kg, which is 27× the load capacity of the simple finger with no electroadhesive (movie S2). Our model predicts an FC of 2.8 kg, which is only 3.6% larger than the measured load capacity. In this demonstration, we observed slight misalignment between the horizontal position of the applied load and the electroadhesive attached to the finger. This caused peeling of the electrodes and explains why the finger's load capacity did not reach the expected value.

Many robotic applications, such as wearables and haptic interfaces, would also benefit from strong electroadhesives to modulate bending stiffness and to resist rotation to provide kinesthetic haptic feedback. As an example, we demonstrated an elbow wearable with an electroadhesive clutch placed on the arm of a mannequin (Fig. 5A). When the electroadhesive was activated at 125 V and the electrodes were lightly pressed into contact, they became adhered. An electroadhesive with L = 40 mm, w = 40 mm, V = 125 V, t = 127 μm, d = 14 μm, and L_f = 24 mm reduced the bend angle of the mannequin′s elbow joint by 17° when loaded under its own weight, resisting a moment of 2.67 N-m. When the clutch was not activated, the electrodes slid past one another, and the elbow freely bent downward. Similarly, we demonstrated a soft finger with an attached high-GSP electroadhesive (Fig. 5B). First, the finger was inflated to 30 kPa, which caused it to easily bend due to its low bending stiffness. In this configuration, the clutch electrodes slid past one another until they were no longer in contact. However, when the clutch was activated at 125 V, the electrodes adhered to one another after being lightly pressed. When the finger was inflated to 30 kPa, the finger′s rotation was substantially reduced due to the increase in bending stiffness resulting from the activated electroadhesive, which increased the finger′s flexural rigidity. Overall, our model can be applied to design strong electroadhesives that notably augment the FC and modulate the stiffness and strength of soft actuators and other robotic systems in both bending and tensile loading scenarios. These were all achieved at 125 V, which is considerably lower than the 300 to 1500 V used in previously reported electroadhesives (*19*–*23*, *25*).

DISCUSSION

We show that a fracture mechanics–based model, and not a parallel plate model, describes the relationship between electroadhesive design and FC. The improved predictive accuracy originates from the model′s ability to assess slip on the basis of the electroadhesion-induced critical energy release rate required to delaminate two electrodes. From this model, a natural set of design variables emerge, which we used to tune the FC by changing the electroadhesive compliance. Our approach differs from previous empirical methods for electroadhesive FC modeling, which accurately predicted the FC of a similar electroadhesive clutch system (*23*) but could not illuminate the driving physical and geometric phenomena that contribute to strength and therefore provided limited insight into design strategies for improving clutch strength, such as the modification of system compliance. Thus, our approach can provide insights into previously unknown clutch materials and architectures that go beyond the single system we are studying because of the derived relationship between clutch stiffness, critical strain energy release rate, and FC. Our approach also allowed us to design strong clutches that do not require substantial amounts of electrostatic force for operation, which was the reason for the performance gains described in this work. Although the fracture-based design approach is key to the performance, the smooth surfaces of the Parylene dielectric layers and the thinness of the electrodes also contribute to the high performance. The smooth surfaces and thinness both promote good contact at the clutch interface, whereas the thinness also helps to reduce the peel stresses at the interface. The clutches that we developed also operated at low voltages with a dielectric of low relative permittivity (κ = 3.1 for Parylene-C) (*44*) and have FCs per unit area that are similar to those of existing clutches at electrostatic pressures that are 1 to 3 orders of magnitude lower (Fig. 6A). Our clutches have a high FC per unit electrostatic force (FC/F_{el}), which is the mechanical FC per input of electrical force and can be viewed as the structural efficiency of the clutch design. Figure 6 (B to D) compares the FC/F_{el} of our clutches to previous work for different FC/A, applied voltage, and absolute FC. The highest-performing clutch we built had an FC per unit electrostatic force of 6.8 at a contact area of 16 cm^2 and 125-V operation (Fig. 6, B and C). Because electroadhesive force capacity scales with V and electrostatic pressure scales with V^2, force capacity per unit electrostatic force scales with $1/V$, which led to our lowest voltage designs (125 V) exhibiting the highest FC/F_{el}. This FC per unit electrostatic force is 63× higher than that of the highest-performing clutch in the literature (*23*). Because electroadhesive FC scales with V and electrostatic pressure scales with V^2, FC per unit electrostatic force scales with $1/V$, which led to our lowest-voltage designs (125 V) exhibiting the highest performance per this metric. Our clutches show absolute FCs that are lower than the best existing clutches (Fig. 6D), because our dielectric's relative permittivity is 10× lower than the dielectric used in prior work (23). The dashed lines in Fig. 6A, however, show the scaling advantage of a high FC/F_{el}. For example, increasing the dielectric constant of our clutches by a factor of 10, while maintaining a FC/F_{el} of 1.5, would increase their FC/A to ~1000 N/cm^2 and absolute FC to ~16kN.

The increases in FC can be achieved with simple changes to the clutch geometry or materials, which allows the application of these improvements to many robotic systems. For example, by changing the clutch′s aspect ratio (L/w) from 4 to $^1/_4$ at a set contact area of 16

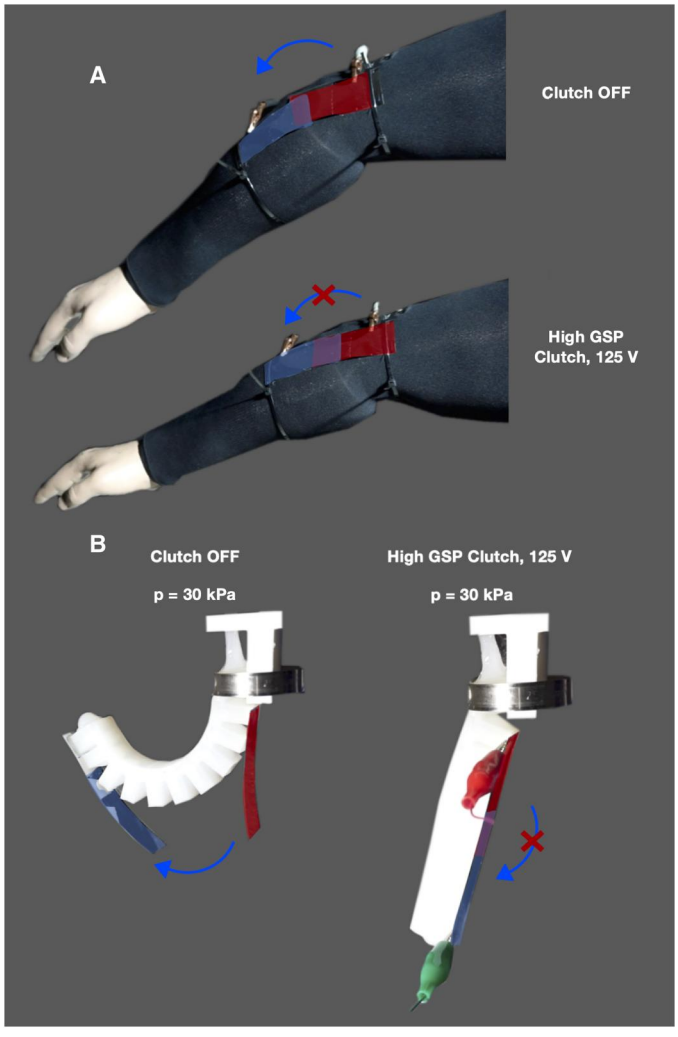

Fig. 5. Using an electroadhesive clutch to resist the bending of an elbow wearable and a soft robotic actuator. (**A**) An elbow wearable with an attached high-GSP clutch activated at 125 V prevented a mannequin forearm from rotating under its own weight (bottom). When 125 V was not applied, the clutch electrodes (red and blue) slid past one another, and the elbow joint freely rotated under the weight of the mannequin arm (top). (**B**) A soft robotic finger with an attached high-GSP clutch bent substantially when inflated to 30 kPa, and the clutch electrodes (red and blue) slid past one another until they were no longer in contact (left). When the clutch was activated at 125 V, it resisted the finger's rotation upon inflation to 30 kPa, whose bending stiffness had increased.

cm^2 and an operating voltage of 200 V, we increased the FC by 2.2×. We demonstrate the value of this with a soft robotic hand that can pick up 27× larger loads when an electroadhesive clutch allows mechanical anchoring of the fingertip to the robot palm. These clutches are easy to manufacture, lightweight, and flexible, and their superior FC/F_{el} over prior work can enable smaller clutches that operate with lower voltages and allow larger changes in material stiffness and strength. The reversible electroadhesion of the presented clutches is also critical in robotic and haptic applications that must undergo repeatable stiffness changes and motions. The fundamental insight into clutch performance solves persistent engineering challenges of incorporating electroadhesive clutches into robotic systems and will enable next-generation wearable and untethered robotic systems such as soft grippers (*45*), morphing sheets (*12*), prosthetics (*46*), orthotics (*47*, *48*), and haptic gloves (*19*, *20*, *49*).

Although the improvements in clutch performance presented here are notable, the accuracy of the model will be limited by the model assumptions. First, because our model assumes that the clutch mechanics is similar to that of a bonded joint, the model may not be applicable when the electrostatic pressure between surfaces is sufficiently low so that there is slip at the contact surfaces. In addition, loading conditions that are very different from the assumed tensile loading could reduce the predictive power of the model, and clutch designs with very small aspect ratios could be susceptible to alignment issues that may reduce the apparent contact area between surfaces. Overall, we found the model to be an excellent predictor of performance for clutches with geometric parameters, such as electrode thickness and aspect ratio, within the range required for most robotic applications where flexibility is desired. Although we have focused on FC, contact area, and operating voltage as critical metrics for electroadhesive clutches, it is important to note that response time, electrode separation, and fatigue life are also key metrics to be considered in clutch design. In addition, delamination between Parylene-C and the aluminum electrode surface was the primary cause of electroadhesive failure. Future work should also consider the influence of the dielectric adhesion on clutch durability.

MATERIALS AND METHODS

Electroadhesive clutch fabrication

An automated blade cutter (Curio, Silhouette Inc.) was used to cut each electrode with a 0.2-mm-thick blade. The electrodes were composed of a 127-μm-thick bi-axially oriented polyethylene terephthalate (BOPET) sheet coated with a thin aluminum film on one side (7538T12, McMaster-Carr Inc.). A chemical vapor deposition system (Specialty Coating Systems, PDS2010) conformally coated the Parylene-C dielectric [poly(chloro-*p*-xylylene)] on the aluminum side of one BOPET electrode. Parylene-C dimer (1.9 g) was vaporized at 175°C, then cleaved into monomers in a pyrolysis furnace at 690°C. The vapor-phase monomer was then polymerized in a deposition chamber at ~25°C, where the clutch electrodes were placed. Kapton tape masked the clutch electrodes to coat only the desired area with dielectric. An Anatech SCE 106 system cleaned all clutch electrodes with oxygen plasma at 30 W for 1 min before coating. To measure the thickness of the dielectric film, we placed 2-cm^2 glass slides (also precleaned with oxygen plasma at 30 W for 1 min) in the coating chamber with the clutch electrodes. A KLA-Tencor P7 stylus profilometer was used to measure the average dielectric thickness to be 14 ± 0.4 μm for all n = 75 electroadhesive specimens.

Tensile testing for electroadhesive FC experiments

To prepare each sample for a tensile test, we used an adhesive (Loctite 409) to attach each electroadhesive specimen to laser-cut acrylic grips to ensure no slipping. A signal generator (Agilent 33220A) applied an AC voltage square wave signal with a frequency of 10 Hz (for a 200-mV amplitude, the voltage fluctuated between +200 and −200 mV), and a high-voltage amplifier (Trek Model 10/10B-HS) amplified the signal by 1000× to its final value. An AC

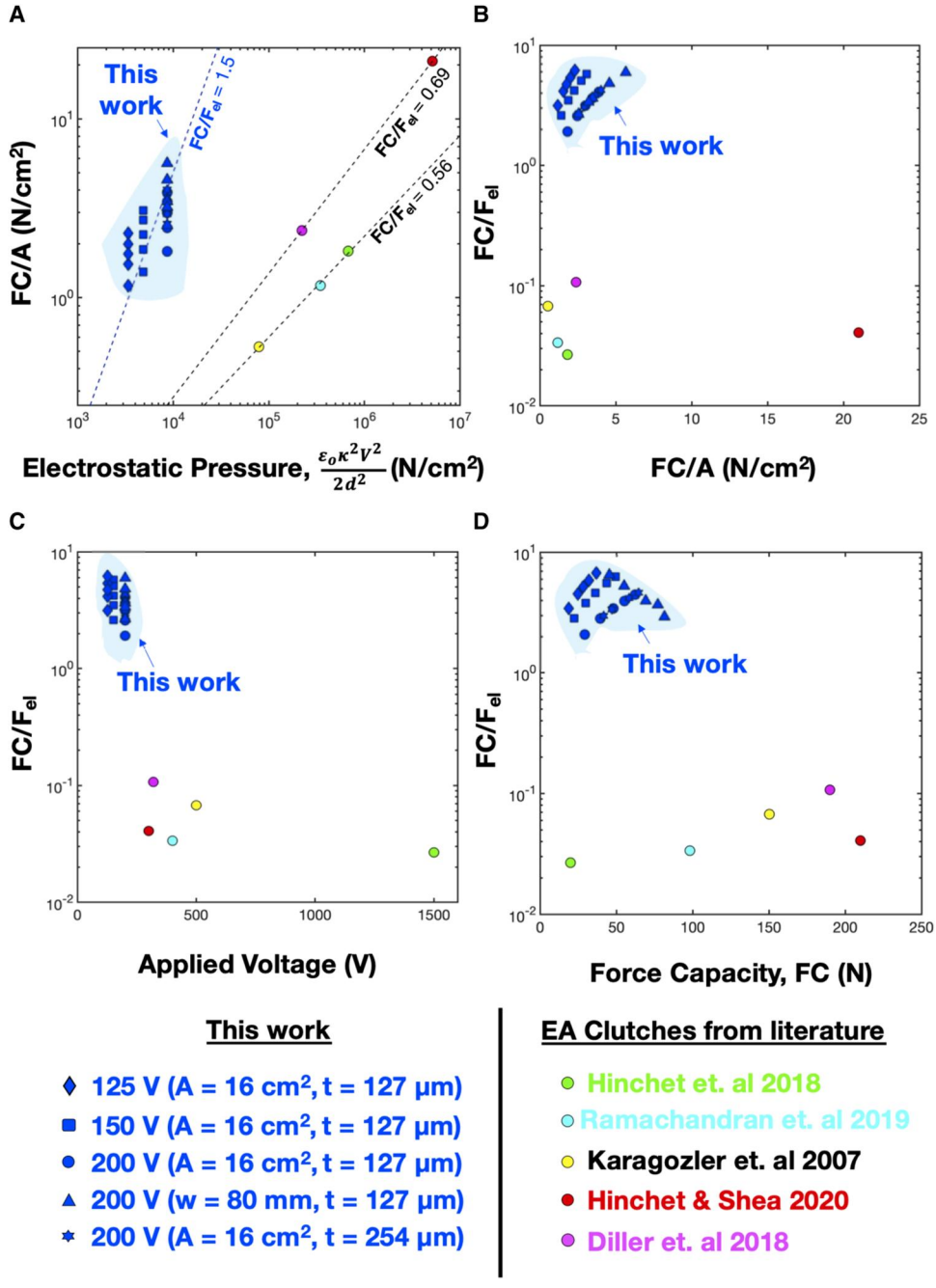

Fig. 6. A comparison of state-of-the-art Coulombic electroadhesive clutches. (**A**) The maximum FC per unit contact area versus total electrostatic pressure at the contact interface. The dashed lines show clutches with a constant FC/F_{el}. (**B-D**) The maximum FC divided by the total electrostatic force applied to the contact interface plotted against (**B**) FC per unit area, (**C**) applied voltage, and (**D**) FC. The data for the clutches from the literature shown here are from (*19*–*22*, *25*).

signal was used to mitigate the effect of space charge buildup in the dielectric. Electrical leads connected the amplifier to the clutch using copper and alligator clips to obtain good electrical contact to the aluminum surface on the polyethylene terephthalate (PET). To characterize the FC of each electroadhesive clutch, we performed uniaxial tensile tests using an MTS Criterion model 43 with a 1-kN load cell with customized tensile grips. The tests were run at a speed of 1 mm min^{-1}. After the voltage was turned on, we manually applied pressure to the overlap region with a 0.8-mm-thick elastomer sheet (Ecoflex 00-30, Smooth-On Inc.) to ensure good contact between the electrode and dielectric surfaces. The tensile setup is pictured in fig. S3.

Materials testing

The modulus of the metallized PET film was determined via uniaxial tensile tests in an MTS Criterion model 43 at a rate of 1 mm min^{-1}. An automated blade cutter (Curio, Silhouette Inc.) was used to cut the PET tensile specimens to type 5 tensile specimens

(ASTM D638). The mean modulus obtained from six PET specimens was 2.3 GPa. A nanoindenter (Hysitron T950) was used to measure the modulus of the Parylene-C film at a variety of indentation depths (200 to 400 nm) with five indents per test. The mean measured modulus of the Parylene-C was 3.6 GPa (fig. S5).

Soft robotic hand fabrication for load capacity tests

For the robotic hand demo, an stereolithography (SLA) three-dimensional printer (Form 3, FormLabs) fabricated molds for Pneu-Net actuators (*50*) and a custom palm, which we designed in Fusion 360 (Autodesk). The fingers were then molded using Dragonskin 10A FAST (Smooth-On Inc.) and cured for 20 min at 70°C. Silicone adhesive (Sil-Poxy, Smooth-On Inc) attached an inextensible paper layer to each finger, along with a flexible inlet tube and one metalized PET clutch electrode, which we cured for 20 min at 70°C.

Load capacity testing of a robotic hand with and without an attached electroadhesive

To test the load capacity of the robotic hand without electroadhesives, we inflated two fingers to 30 kPa and loaded them with a bag containing one 0.2-kg apple, which it held without dropping. An attached pressure sensor (Sparkfun Qwicc Micropressure Sensor, Sparkfun) measured the pressure value. Next, we loaded the same fingers with a full 1.8-kg bag of apples, which they could not hold. To test the load capacity of a single soft finger with an electroadhesive attached, we attached one electrode to the palm with double-sided foam tape (VHB 4910, 3M). After inflating the finger, we activated the clutch at 125 V, mechanically anchoring the finger to the palm. We loaded the finger with the 1.8-kg bag, which it could successfully hold. This demonstration can be found in movie S1. To test the FC of a finger with w = 20 mm and L = 80 mm clutch attached, we inflated it to 30 kPa and then manually pressed the electrodes into contact. At this point, we added weight to the finger until the electrodes detached. We repeated the same procedure for a soft finger with an electroadhesive with increased GSP (w = 40 mm and L = 40 mm). We attached weights to the finger using two zip ties and an S hook. The setup is shown in fig. S4, and a video of this demonstration is provided in movie S2.

Elbow wearable demonstration with and without an activated electroadhesive

To test the ability of an electroadhesive clutch to prevent the bending of an elbow wearable, we attached the electrodes of an increased GSP clutch (w = 40 mm and L = 40 mm) to a cotton arm sleeve with cyanoacrylate glue. We then placed the elbow sleeve on the arm of a mannequin. When the clutch was not activated, we loaded the mannequin arm under its own weight, causing the forearm to deflect substantially, because the elbow was free to rotate. When we activated the clutch at 125 V and lightly pressed down on the contacting electrodes on the outside of the elbow joint, they adhered. When the arm was then loaded under its own weight, it deflected by a reduced amount compared with the initial, nonactivated deflection (movie S3).

Soft bending actuator demonstration with and without an activated electroadhesive

To test the ability of an electroadhesive clutch to prevent the bending of a soft pneumatic bending actuator, we attached the electrodes of an increased GSP clutch (w = 40 mm and L = 40 mm) to the back of a Pneu-Net finger with silicone adhesive (Sil-Poxy). A custom fixture held the finger in place, oriented downward with its air inlet tube facing up. When the clutch was not activated, we inflated the finger to 30 kPa, causing notable bending because the finger was unobstructed. When we activated the clutch at 125 V and lightly pressed down on the contacting electrodes on the extensible side of the finger, they adhered. When the finger was once again inflated to 30 kPa, its bending angle was notably reduced compared with the initial, nonactivated state (movie S3).

Supplementary Materials

This PDF file includes:
Figs. S1 to S5

Other Supplementary Material for this manuscript includes the following:
Movies S1 to S3

REFERENCES AND NOTES

1. E. J. Rouse, L. M. Mooney, H. M. Herr, Clutchable series-elastic actuator: Implications for prosthetic knee design. *Int. J. Robot. Res.* **33**, 1611–1625 (2014).
2. K. C. Galloway, J. E. Clark, D. E. Koditschek, Variable stiffness legs for robust, efficient, and stable dynamic running. *J. Mech. Robot.* **5**, 011009 (2013).
3. M. Taghavi, T. Helps, J. Rossiter, Electro-ribbon actuators and electro-origami robots. *Sci. Robot.* **3**, eaau9795 (2018).
4. S. Mintchev, J. Shintake, D. Floreano, Bioinspired dual-stiffness origami. *Sci. Robot.* **3**, eaau0275 (2018).
5. S. Miyashita, S. Guitron, S. Li, D. Rus, Robotic metamorphosis by origami exoskeletons. *Sci. Robot.* **2**, eaao4369 (2017).
6. K. A. Witte, P. Fiers, A. L. Sheets-Singer, S. H. Collins, Improving the energy economy of human running with powered and unpowered ankle exoskeleton assistance. *Sci. Robot.* **5**, eaay9108 (2020).
7. M. Plooij, G. Mathijssen, P. Cherelle, D. Lefeber, B. Vanderborght, Lock your robot: A review of locking devices in robotics. *IEEE Robot. Autom. Mag.* **22**, 106–117 (2015).
8. S. H. Collins, M. B. Wiggin, G. S. Sawicki, Reducing the energy cost of human walking using an unpowered exoskeleton. *Nature* **522**, 212–215 (2015).
9. K. Spanner, B. Koc, Piezoelectric motors, an overview. *Actuators* **5**, 6 (2016).
10. J. Nikitczuk, B. Weinberg, P. K. Canavan, C. Mavroidis, Active knee rehabilitation orthotic device with variable damping characteristics implemented via an electrorheological fluid. *IEEEASME Trans. Mechatron.* **15**, 952–960 (2010).
11. A. S. Shafer, M. R. Kermani, Design and validation of a magneto-rheological clutch for practical control applications in human-friendly manipulation, in *Proceedings of the 2011 IEEE International Conference on Robotics and Automation* (IEEE, 2011).
12. J. H. Pikul, S. Li, H. Bai, R. T. Hanlon, I. Cohen, R. F. Shepherd, Stretchable surfaces with programmable 3D texture morphing for synthetic camouflaging skins. *Science* **358**, 210–214 (2017).
13. Q. Zhong, J. Zhu, F. E. Fish, S. J. Kerr, A. M. Downs, H. Bart-Smith, D. B. Quinn, Tunable stiffness enables fast and efficient swimming in fish-like robots. *Sci. Robot.* **6**, eabe4088 (2021).
14. E. Palleau, D. Morales, M. D. Dickey, O. D. Velev, Reversible patterning and actuation of hydrogels by electrically assisted ionoprinting. *Nat. Commun.* **4**, 2257 (2013).
15. D. J. Levine, K. T. Turner, J. H. Pikul, Materials with electroprogrammable stiffness. *Adv. Mater.* **33**, 2007952 (2021).
16. M. Manti, V. Cacucciolo, M. Cianchetti, Stiffening in soft robotics: A review of the state of the art. *IEEE Robot. Autom. Mag.* **23**, 93–106 (2016).
17. J. Guo, J. Leng, J. Rossiter, Electroadhesion technologies for robotics: A comprehensive review. *IEEE Trans. Robot.* , 313–327 (2019).
18. A. Johnsen, K. Rahbek, A physical phenomenon and its applications to telegraphy, telephony, etc. *J. Inst. Electr. Eng.* **61**, 713–725 (1923).
19. R. Hinchet, V. Vechev, H. Shea, O. Hilliges, DextrES: Wearable haptic feedback for grasping in VR via a thin form-factor electrostatic brake, in *Proceedings of the 31st Annual ACM Symposium on User Interface Software and Technology - UIST '18* (ACM Press, Berlin, Germany, 2018), pp. 901–912; http://dl.acm.org/citation.cfm?doid=3242587.3242657.

20. R. Hinchet, H. Shea, High force density textile electrostatic clutch. *Adv. Mater. Technol.* **5**, 1900895 (2020).
21. V. Ramachandran, J. Shintake, D. Floreano, All-fabric wearable electroadhesive clutch. *Adv. Mater. Technol.* **4**, 1800313 (2019).
22. S. Diller, C. Majidi, S. H. Collins, A lightweight, low-power electroadhesive clutch and spring for exoskeleton actuation, in *Proceedings of the 2016 IEEE International Conference on Robotics and Automation (ICRA)* (IEEE, 2016), pp. 682–689.
23. S. B. Diller, S. H. Collins, C. Majidi, The effects of electroadhesive clutch design parameters on performance characteristics. *J. Intell. Mater. Syst. Struct.* **29**, 3804–3828 (2018).
24. H. Imamura, K. Kadooka, M. Taya, A variable stiffness dielectric elastomer actuator based on electrostatic chucking. *Soft Matter* **13**, 3440–3448 (2017).
25. M. E. Karagozler, J. D. Campbell, G. K. Fedder, S. C. Goldstein, M. P. Weller, B. W. Yoon, Electrostatic latching for inter-module adhesion, power transfer, and communication in modular robots, in *Proceedings of the 2007 IEEE/RSJ International Conference on Intelligent Robots and Systems* (IEEE, 2007), pp. 2779–2786.
26. T. Wang, J. Zhang, Y. Li, J. Hong, M. Y. Wang, Electrostatic layer jamming variable stiffness for soft robotics. *IEEEASME Trans. Mechatron.* **24**, 424–433 (2019).
27. A. S. Chen, S. Bergbreiter, A comparison of critical shear force in low-voltage, all-polymer electroadhesives to a basic friction model. *Smart Mater. Struct.* **26**, 025028 (2017).
28. M. D. Bartlett, A. B. Croll, D. R. King, B. M. Paret, D. J. Irschick, A. J. Crosby, Looking beyond fibrillar features to scale gecko-like adhesion. *Adv. Mater.* **24**, 1078–1083 (2012).
29. D. R. King, A. J. Crosby, Optimizing adhesive design by understanding compliance. *ACS Appl. Mater. Interfaces* **7**, 27771–27781 (2015).
30. C. A. Gilman, M. J. Imburgia, M. D. Bartlett, D. R. King, A. J. Crosby, D. J. Irschick, Geckos as springs: Mechanics explain across-species scaling of adhesion. *PLOS ONE* **10**, e0134604 (2015).
31. A. B. Croll, N. Hosseini, M. D. Bartlett, Switchable adhesives for multifunctional interfaces. *Adv. Mater. Technol.* **4**, 1900193 (2019).
32. M. D. Bartlett, A. B. Croll, A. J. Crosby, Designing bio-inspired adhesives for shear loading: From simple structures to complex patterns. *Adv. Funct. Mater.* **22**, 4985–4992 (2012).
33. M. D. Bartlett, A. J. Crosby, High capacity, easy release adhesives from renewable materials. *Adv. Mater.* **26**, 3405–3409 (2014).
34. M. D. Bartlett, A. J. Crosby, Scaling normal adhesion force capacity with a generalized parameter. *Langmuir* **29**, 11022–11027 (2013).
35. M. Goland, E. Reissner, The stresses in cemented joints. *J. Appl. Mech.* **11**, A17–A27 (1944).
36. S. Kumar, B. L. Wardle, M. F. Arif, Strength and performance enhancement of bonded joints by spatial tailoring of adhesive compliance via 3D printing. *ACS Appl. Mater. Interfaces* **9**, 884–891 (2017).
37. S. Kumar, B. L. Wardle, M. F. Arif, J. Ubaid, Stress reduction of 3D printed compliance-tailored multilayers. *Adv. Eng. Mater.* **20**, 1700883 (2018).
38. J. Ubaid, B. L. Wardle, S. Kumar, Strength and performance enhancement of multilayers by spatial tailoring of adherend compliance and morphology via multimaterial jetting additive manufacturing. *Sci. Rep.* **8**, 13592 (2018).
39. S. Ponce, J. Bico, B. Roman, Effect of friction on the peeling test at zero-degrees. *Soft Matter* **11**, 9281–9290 (2015).
40. V. Cacucciolo, H. Shea, G. Carbone, Peeling in electroadhesion soft grippers. *Extreme Mech. Lett.* **50**, 101529 (2022).
41. H. J. Kim, L. Paquin, C. W. Barney, S. So, B. Chen, Z. Suo, A. J. Crosby, R. C. Hayward, Low-voltage reversible electroadhesion of ionoelastomer junctions. *Adv. Mater.* **32**, 2000600 (2020).
42. A. R. Mojdehi, D. P. Holmes, D. A. Dillard, Revisiting the generalized scaling law for adhesion: Role of compliance and extension to progressive failure. *Soft Matter* **13**, 7529–7536 (2017).
43. J. Shintake, V. Cacucciolo, D. Floreano, H. Shea, Soft robotic grippers. *Adv. Mater.* **30**, 1707035 (2018).
44. W. F. Beach, in *Kirk-Othmer Encyclopedia of Chemical Technology* (American Cancer Society, 2000); http://onlinelibrary.wiley.com/doi/abs/10.1002/0471238961.2425122502050103.a01.
45. N. R. Sinatra, C. B. Teeple, D. M. Vogt, K. K. Parker, D. F. Gruber, R. J. Wood, Ultragentle manipulation of delicate structures using a soft robotic gripper. *Sci. Robot.* **4**, eaax5425 (2019).
46. K. W. O'Brien, P. A. Xu, D. J. Levine, C. A. Aubin, H.-J. Yang, M. F. Xiao, L. W. Wiesner, R. F. Shepherd, Elastomeric passive transmission for autonomous force-velocity adaptation applied to 3D-printed prosthetics. *Sci. Robot.* **3**, eaau5543 (2018).
47. H. Zhao, J. Jalving, R. Huang, R. Knepper, A. Ruina, R. Shepherd, A helping hand: Soft orthosis with integrated optical strain sensors and EMG control. *IEEE Robot. Autom. Mag.* **23**, 55–64 (2016).
48. P. Polygerinos, Z. Wang, K. C. Galloway, R. J. Wood, C. J. Walsh, Soft robotic glove for combined assistance and at-home rehabilitation. *Robot. Auton. Syst.* **73**, 135–143 (2015).
49. E. Leroy, R. Hinchet, H. Shea, Multimode hydraulically amplified electrostatic actuators for wearable haptics. *Adv. Mater.* **32**, 2002564 (2020).
50. B. Mosadegh, P. Polygerinos, C. Keplinger, S. Wennstedt, R. F. Shepherd, U. Gupta, J. Shim, K. Bertoldi, C. J. Walsh, G. M. Whitesides, Pneumatic networks for soft robotics that actuate rapidly. *Adv. Funct. Mater.* **24**, 2163–2170 (2014).

Acknowledgments: D.J.L. would like to thank G. Campbell for feedback and support over the course of this project and S. Fulco for assistance with nanoindentation experiments. **Funding:** D.J.L. was partially supported by a Department of Education GAANN fellowship grant number P200A160282 to the Department of Mechanical Engineering and Applied Mechanics at the University of Pennsylvania. D.J.L. and J.H.P. were partially supported by the NSF Emerging Frontiers in Research and Innovation (EFRI) award #1935294. D.J.L. and K.T.T. were partially supported by the NSF Robotics Initiative, award no. 1830475. This research is funded in part by the Gordon and Betty Moore Foundation through grant GBMF9691 to J.H.P. This work was performed in part at the Singh Center for Nanotechnology, a node in the National Nanotechnology Coordinated Infrastructure (NNCI) network, which is supported by the NSF under grant NNCI-1542153. **Author contributions:** D.J.L., K.T.T., and J.H.P. conceived the research and the device concepts. D.J.L. designed and conducted experiments, manufactured the electroadhesives, performed the analytical modeling, collected and analyzed the data, interpreted the results, and wrote the manuscript. G.M.I. and R.D.R. designed and conducted experiments. K.T.T. and J.H.P. supervised the research, designed experiments, interpreted the results, and edited the manuscript. **Competing interests:** The authors declare that they have no competing interests. **Data and materials availability:** All data needed to evaluate the conclusions in the paper are present in the paper or the Supplementary Materials. The data for this study have been deposited in the Materials Data Facility database.

Submitted 20 January 2022
Accepted 18 August 2022
Published 30 November 2022
10.1126/scirobotics.abo2179

Science Robotics

A mechanics-based approach to realize high–force capacity electroadhesives for robots

David J. Levine, Gokulanand M. Iyer, R. Daelan Roosa, Kevin T. Turner, and James H. Pikul

Sci. Robot. **7** (72), eabo2179. DOI: 10.1126/scirobotics.abo2179

Science Robotics (ISSN 2470-9476) is published by the American Association for the Advancement of Science. 1200 New York Avenue NW, Washington, DC 20005. The title *Science Robotics* is a registered trademark of AAAS.